ACS Infectious Diseases

pubs.acs.org/journal/aidcbc

Article

Nanobody-Based Bispecific Neutralizer for Shiga Toxin-Producing *E. coli*

Zhongkai Lu, Zhicheng Liu, Xia Li, Xinfang Qin, Haofei Hong, Zhifang Zhou, Roland J. Pieters,* Jie Shi,* and Zhimeng Wu*

Cite This: *ACS Infect. Dis.* 2022, 8, 321−329

Read Online

ACCESS | Metrics & More | Article Recommendations | Supporting Information

ABSTRACT: Currently, no specific therapeutics are available for foodborne Shiga toxin-producing *Escherichia coli* (STEC) infections that cause severe gastroenteritis and life-threatening complications of hemolytic uremic syndrome (HUS). As STEC attachment to intestinal epithelium might increase the host absorption of Shiga toxins and severity of the disease, we were inspired to develop a bispecific neutralizer capable of blocking its Shiga toxin and adhesin intimin simultaneously. Two nanobodies against the B subunit of Shiga toxin 2 (Stx2B) and the C terminus of Intimin (IntC280) were genetically fused together as the bispecific neutralizer, and it can be efficiently produced in a conventional *E. coli* expression system. We demonstrated that each of the nanobody modules in the bispecific format showed increased antigen binding capability and was able to functionally neutralize the binding of Stx2B or IntC280 to the respective host receptors even in the presence of the two virulence factors together. Moreover, the bispecific neutralizer was relatively stable to harsh storage conditions and gastrointestinal pH extremes. Taking into account its easy and economical production and superior pharmaceutical properties, we believe that a nanobody-based bispecific neutralizer would be more favorable and practical to be developed as a therapeutic to fight STEC in the developing world.

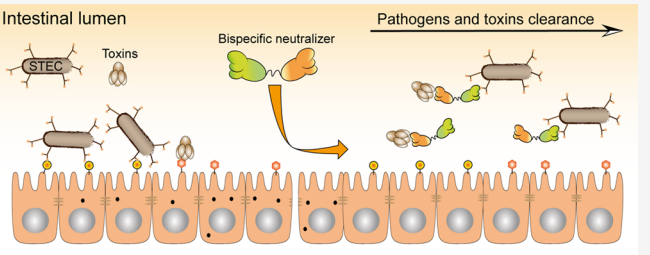

KEYWORDS: *bispecific nanobody, STEC, Shiga toxin, intimin, Gb3*

Shiga toxin-producing *Escherichia coli* (STEC) is an infectious enteric pathogen that causes severe gastroenteritis worldwide. Although STEC infected cases are often sporadic and occur on a small scale, STEC also causes large outbreaks due to its highly infectious nature.[1−4] The symptoms of STEC infections are mostly severe stomach cramps and bloody diarrhea, but it was estimated that 6−25% of patients developed life-threatening complications known as hemolytic uremic syndrome (HUS), which is characterized by hemolytic anemia, thrombocytopenia, and acute kidney injury.[5−7] Currently, no specific preventions and therapeutics against STEC infections are available for clinical use, and early drug development has been mostly focused on neutralizing its disease-causing virulence factors including Shiga toxins.[8,9]

Shiga toxins are the main virulence factors that drive organ damage and cause complications of HUS in STEC-infected people.[10,11] Shiga toxin 1 and 2 are the most common subtypes associated with disease, but more subvariants have also been identified.[12] Both subtypes of Shiga toxins share a common AB_5 architecture of a subunit A and a pentamer subunit B. The B subunits are responsible for targeting host cells through the receptor globotriaosylceramide (Gb3), which is expressed on the surface of several types of cells including endothelium cells of the gut, kidney, brain, as well as tubular and mesangial cells inside the kidney.[10] After entering the host cells, the A subunit matures as an active *N*-glycosidase that cleaves an adenine from the 28S RNA in the ribosome and interferes with proteins synthesis which results in cell death.[13] With respect to neutralizing Shiga toxin-caused cytotoxicity, most attempts have been focused on developing Gb3 competitive inhibitors, for example multivalent neutralizers by displaying the functional carbohydrate part of Gb3 or its analogues on a probiotic, nanoparticle, polymer, or multivalent scaffold.[14−18] Passive immunization including conventional antibodies and recombinant antibody fragments such as ScFv and Fab have also been developed to target and neutralize Shiga toxins.[19−21] Interestingly, nanobodies, the variable domain of camelid heavy chain antibody, against Stx1 and Stx2 as neutralizer also showed therapeutic potential for HUS.[22−24] Inherent advantages of a nanobody over conventional antibody such as easy production, high stability, and tolerance to modifications have made it a promising alternative for targeted-drug development targeting infectious diseases.[25−28]

Received: August 30, 2021
Published: January 11, 2022

Another pathogenicity of STEC additionally comes from its type III secretion system (T3SS) and the secreted effector proteins that mediate the intimate attachment and effacement of host enteric cells. The tight attachment of the bacterium to host enteric cells partially relies on the specific interaction of its adhesin intimin and the T3SS translocated-intimin receptor (Tir) on the host cell membrane.[29] A recently reported nanobody against Tir was shown to be able to inhibit enterohemorrhagic *E. coli* attachment and colonization by blocking Intimin-Tir interactions, thus indicating the therapeutic possibility by targeting this interaction.[30] In addition, a virulence profiling study of the 2011 European outbreak strain suggested that the adherence of this strain to intestinal epithelium cells might increase the absorption of Shiga toxins and progression and severity of HUS.[31] However, to date, no efforts and attempts have been made to study a bispecific or synergistic strategy to target STEC attachment and its toxins simultaneously.

In the present work, as inspired by the hints that STEC attachment increases host Shiga toxin absorptions, we report the construction and *in vitro* evaluation of a bispecific neutralizer consisting of two existing nanobodies against Shiga toxin and intimin, respectively. We demonstrated that each of the modules in the bispecific construct showed increased antigen binding capability compared to the respective monospecific nanobody and that the bispecific construct was able to functionally block the binding of Shiga toxin or intimin to their respective receptors when these virulence factors were even present simultaneously. Taking into consideration the easy and economical production, superior pharmaceutical properties, and high stability of this construct, we believe that introducing this bispecific concept of nanobodies for drug development should bring practical benefits into the fight against STEC infections in the developing world.

RESULTS AND DISCUSSION

Fabrication of the Bispecific Neutralizer. To obtain a construct capable of simultaneously neutralizing the binding of Shiga toxin and intimin to their respective host receptors (Figure 1A), two reported nanobodies against the B subunit of Shiga toxin 2 (Stx2B) and C terminus of intimin (IntC280), i.e., Nb113 and IB10, were chosen to fabricate a bispecific nanobody.[24,32] To this end, two nanobodies were genetically fused through a $(G_4S)_3$ linker with NB113 at the N terminus and IB10 at the C terminus, with a hope that each individual nanobody module can retain its full antigen binding capability (Figure 1B). For the sake of brevity, the recombinant bispecific Nanobody for Shiga toxin and Intimin was hereinafter referred to as siNb. The codon-optimized gene for coding siNb was cloned into a pET-22b vector for expression using the *E. coli* Bl21 (DE3) strain. After straightforward purification using a nickel affinity protein purification column, eluted proteins were analyzed by using SDS-PAGE. As shown in Figure 1C, a single protein band was detected from elution fractions in Lane 5−7 with a size consistent with the theoretical molecule weight for siNb of 28.49 kDa and it was further confirmed as siNb by Western blot analysis using antibodies against His-tag and the nanobody as well (Figure 1D). All the corresponding fractions were desalted and concentrated, resulting in pure siNb with a final yield of 4.5 mg/L. The resultant siNb was also characterized by size-exclusion chromatography (SEC) analysis and high-resolution mass spectrometry, which indicated a

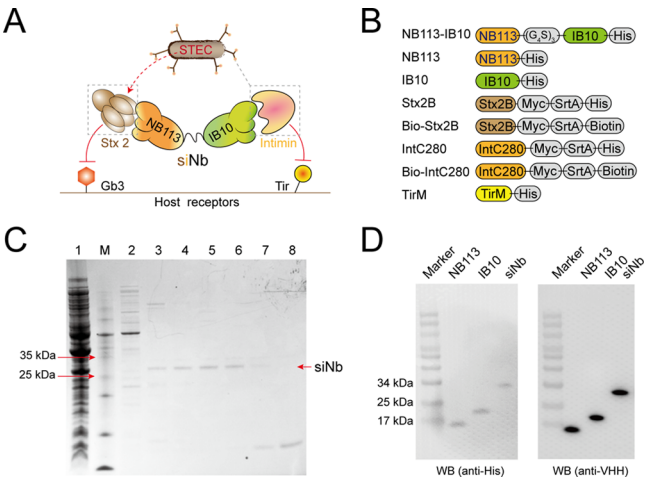

Figure 1. Fabrication and characterization of the bispecific neutralizer siNb. (A) Schematic depiction of the bispecific neutralizer. (B) Primary architectures of the bispecific neutralizer and other relevant proteins. (C) SDS-PAGE analysis of the purified bispecific neutralizer. Lane 1: lysate, Lane M: marker, Lane 2 and 3: washing buffer with 50 mM or 75 mM imidazole, and Lane 4−8: elution buffer with 100, 175, 250, 500, 500 mM imidazole. (D) The bispecific nanobody together with two monospecific nanobodies were analyzed by using Western blot with antibodies against His-tag (left panel) and nanobody (right panel).

molecule weight of siNb well in agreement with the calculated value (Figure S1 and S2). In addition, monospecific nanobodies and all the relevant proteins were prepared accordingly for the mentioned characterization of siNb (Figure 1B and Figure S3). It is important to note that the production of such a construct at low cost and high yield using a common *E. coli* system would be a favorable advantage to meet the requirement for quick production of preventives and biotherapeutics in response to an STEC outbreak challenge.

Antigen Binding Affinity of the Bispecific Neutralizer. With this construct in hand, we then tested its binding capability to Stx2B and IntC280, respectively. To rule out the possibility of an unfavorable effect of protein fusion on its affinity, we first compared the antigen-binding affinity of each monospecific module in siNb with that of each monospecific nanobody individually expressed (Figure 2A). For this purpose, Stx2B or IntC280 without His-tag were immobilized on a microplate for an ELISA assay and the binding of nanobodies (His-tagged) was determined accordingly using HisProbe-HRP. Surprisingly, the binding affinity of NB113 portion in siNb to Stx2B turned out to be 8.7 times higher than that of the monospecific nanobody NB113 (Figure 2B), while the binding affinity of the IB10 portion in siNb was 2.7-fold of that of the monospecific nanobody IB10 (Figure 2C). This affinity increasement of siNb might not come from the cross-reactivity of each nanobody module, because no significant binding of each monospecific nanobody to the irrelevant antigen can be detected even at high concentrations up to 4 μM (Figure S4).

We next determined whether each of the modules in this bispecific construct can independently function in the presence of two antigens simultaneously. To achieve this purpose in an ELISA type assay, Stx2B without His tag was first coated on the plate and likewise the binding of bio-Int280 (biotin labeled) mediated by siNb was determined using a streptavidin-conjugated HRP, and vice versa (Figure 2D). As

https://doi.org/10.1021/acsinfecdis.1c00456
ACS Infect. Dis. 2022, 8, 321−329

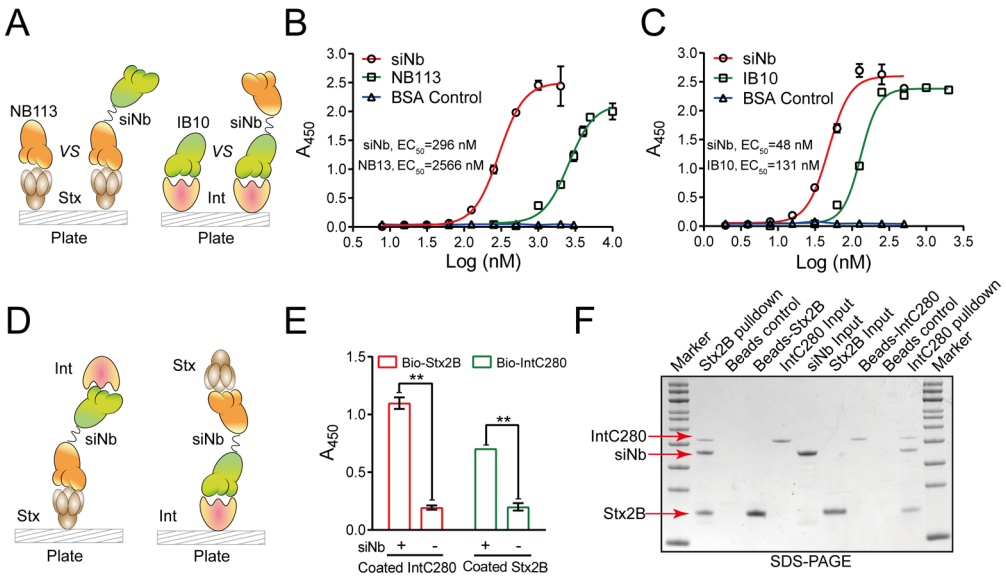

Figure 2. Antigens binding by the bispecific neutralizer. (A) Schematic depiction of ELISA type assay for individual antigen binding. (B) Affinity comparison of NB113-IB10 and NB113 binding to Stx2B as described in left panel of (A). (C) Affinity comparison of NB113-IB10 and IB10 binding to IntC280. (D) Schematic depiction of ELISA type assay for simultaneous antigen binding. ELISA (E) and pull-down analysis (F) of the bispecific construct binding to two Stx2B and IntC280 simultaneously.

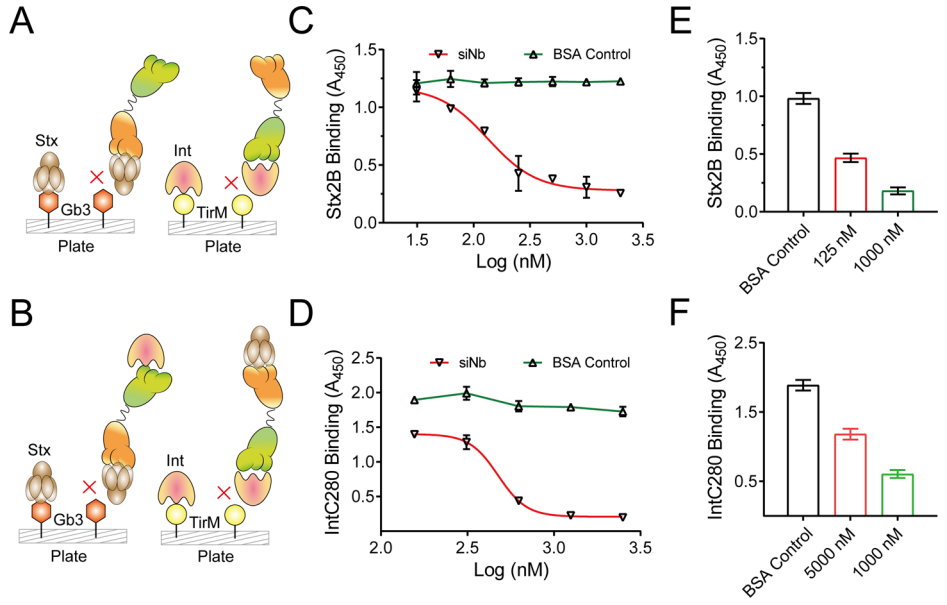

Figure 3. Functional neutralization of Shiga toxin and intimin by the bispecific neutralizer. (A) Schematic depiction of the function assay for Shiga toxin neutralization. (B) Schematic depiction of the function assay for IntC280 neutralization. (C) Shiga toxin neutralization by various concentrations of siNb. (D) Int280 neutralization by various concentration of siNb. (E) Stx2B neutralization by siNb in the presence of IntC280 (6 μM). (F) IntC280 neutralization by siNb in the presence of Stx2B (19 μM).

shown in Figure 2E, whether it was Stx2B or Int280 immobilized, the formation of a ternary complex can be determined in the presence of the siNb at the concentrations indicated, but no significant signal accounting for this complex can be detected in the controls without siNb. In the same vein, this ternary complex of siNb and two types of antigens was further validated in a pull-down assay where one of the antigens with biotin was immobilized on streptavidin magnetic beads and the bound proteins after incubation were visualized using SDS-PAGE. As shown in Figure 2F, three bands corresponding to Stx2B, siNb, and IntC280 can be detected from the pull-down samples, indicating the formation of the ternary complex. The binding of siNb to the immobilized Stx2B was further compared with that in the presence of free Int280 using the above ELISA assay and vice versa (Figure S5). Under both conditions, siNb did not show significant difference in its ability to bind to each immobilized antigen, which further excluded the possibility of cross-reactivity from each nanobody module. We speculated that protein-fusion might stabilize the bispecific construct in conformation, and thus siNb showed the increased binding ability to each antigen.

Taken together, these results demonstrated that the bispecific construct retained the individual function of each nanobody module with even enhanced antigen binding

https://doi.org/10.1021/acsinfecdis.1c00456
ACS Infect. Dis. 2022, 8, 321−329

capability. Most importantly, it can bind to both antigens simultaneously as we initially hoped for such a construct.

Functional Blocking of Shiga Toxins and Intimin by the Bispecific Neutralizer. Next, we tested the ability of this bispecific construct for functionally neutralizing Shiga toxin and Intimin. Inhibition of Stx2B binding to its receptor Gb3 trisaccharide was determined by using a functional ELISA type assay as we described previously.[15] The Gb3 construct was immobilized on the plate and the Bio-Stx2B binding to Gb3 was determined in the presence or absence of siNb (Figure 3A left panel, and Figure S6A). As shown in Figure 3C, the addition of BSA as a control had no effect on the Bio-Stx2B binding, while introduction of siNb blocked that in a concentration dependent manner, with an EC_{50} of 133 nM. Likewise, a similar functional assay was developed to determine the effect of siNb on the binding of IntC280 to TirM as depicted in the right panel of Figure 3A. Recombinant TirM was coated on the plate and the binding of Bio-Int280 was determined in the presence or absence of siNb (Figure S6B). Again, nonspecific control BSA did not significantly interfere with the binding of Bio-Int280 to immobilized TirM and as expected concentration dependent inhibition of this interaction was seen in the presence of siNb, resulting in an EC_{50} of 475 nM (Figure 3D).

Although the simultaneous binding of siNb to two different antigens was well demonstrated above, we here continued to test its neutralization ability in the presence of two antigens simultaneously. The above two functional assays were further performed in the simultaneous presence of the two different antigens and the binding of each antigen to its corresponding receptor was determined respectively as shown in Figure 3B. As shown in Figure 3E and 3F, the addition of siNb at the EC_{50} concentration of each module inhibited the antigens binding to respective receptors by 50%. As free Shiga toxins were also detected in blood circulation of infected patients, the ability of siNb to neutralize stx2B was also determined in serum simulation (Figure S7). These data suggest that the bispecific nanobody as bifunctional neutralizer is capable of blocking the binding of Shiga toxin and intimin to their respective receptors.

The Bispecific Neutralizer Blocked Stx2B Attachment to Gb3 Expressing Colorectal Cells. We then studied the ability of this bispecific neutralizer to block the binding of stx2B to Gb3 receptor using human cells. An array of cancer cell lines was scanned for Stx2B binding using a flow cytometry analysis (Figure S8) and colorectal cell line HT29 expressing the highest Gb3 level was finally chosen as a model for the subsequent study (Figure S9A and S9B). As expected, treating the cells with increasing concentrations of siNb showed concentration dependent inhibition on Stx2B (500 nM) binding to the cells and complete inhibition was seen when it reached at 1 μM (Figure 4 and Figure S9C and S9D). The presence of high concentration of IntC280 consistently did not show unfavorable effect on this activity of siNb (Figure 4). Interestingly, siNb showed more potent Stx2B inhibition than the monospecific module Nb113, which can be attributed to the enhanced binding capability of siNb to Stx2B as we observed (Figure 2B). In addition, an immuno-cytochemical analysis was performed to visualize the inhibition of Stx2B binding to HT29 cells. As shown in Figure 5, Stx2B labeled by fluorescent anti-MYC antibody (green) was clustered on HT29 cell surface in the absence of siNb, but this clustering of Stx2B was significantly reduced by the addition of siNb at 250 nM and it was completely invisible when 500 nM of siNb was given. The above data demonstrated that the bispecific neutralizer can block the attachment of Stx2B onto colorectal cells and it should also be applicable to other types of cells expressing such Gb3 receptors.

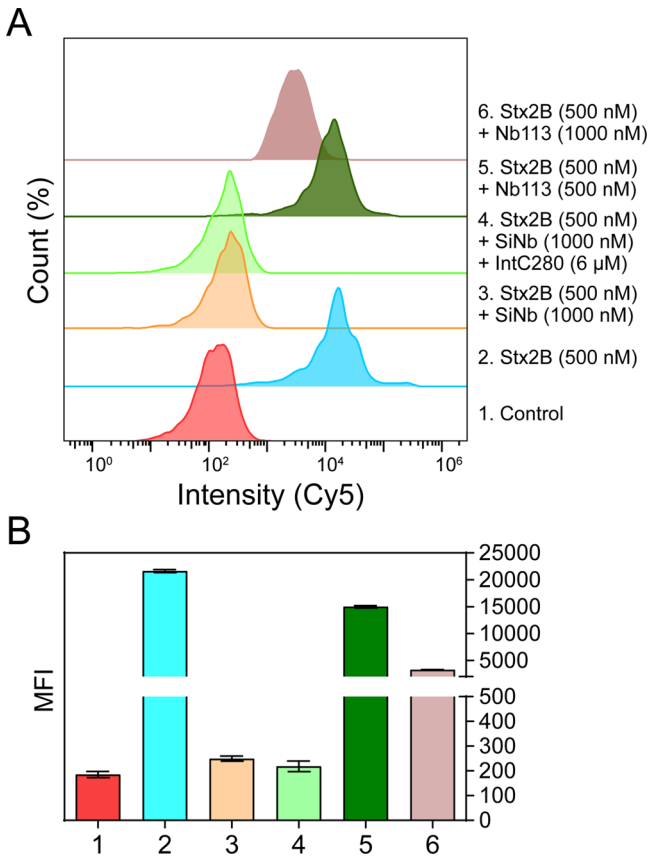

Figure 4. Flow cytometry analysis of the inhibitory effect of siNb on Stx2B attachment to HT29 cells. (A) HT29 cells were treated with Stx2B or in combination with either siNb or Nb113, and the bound Stx2B was labeled and counted by a flow cytometer using an anti-MYC primary antibody and a Cy5-conjugated secondary antibody. (B) The mean fluorescence intensity (MFI) quantification of the result of (A). Treatment without Stx2B was used a negative control.

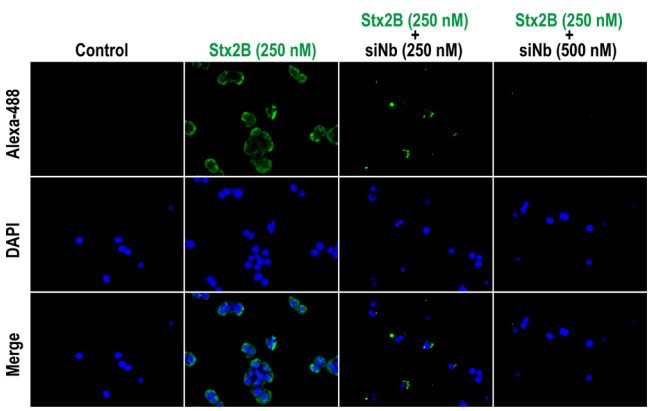

Figure 5. Immuno-cytochemical analysis of the inhibitory effect of siNb on Stx2B attachment to HT29 cells. HT29 cells were treated with Stx2B with or without siNb, and the attachment of Stx2B was labeled and visualized under a fluorescent microscopy using an anti-MYC primary antibody and an Aleaxa-488-conjugated secondary antibody. Treatment without Stx2B was used as a negative control.

https://doi.org/10.1021/acsinfecdis.1c00456
ACS Infect. Dis. 2022, 8, 321−329

The Stability of the Bispecific Neutralizer to Storage Conditions, Lyophilization, and pH. The high stability under harsh conditions might be more desirable for developing biopreventives and biotherapeutics against STEC infections as the cases are often sporadic and the cold-chain transportation together with strict storage conditions of unstable drugs inevitably increases the cost especially in developing countries. In this regard, we next tested the stability of the bispecific neutralizer to freezing-thaw, long-term storage, lyophilization. For the freezing-thaw stability of siNb, a total of three cycles of freezing-thaw did not cause significant protein degradation and reduction of its binding capability to both stx2B and IntC280 (Figure 6A).

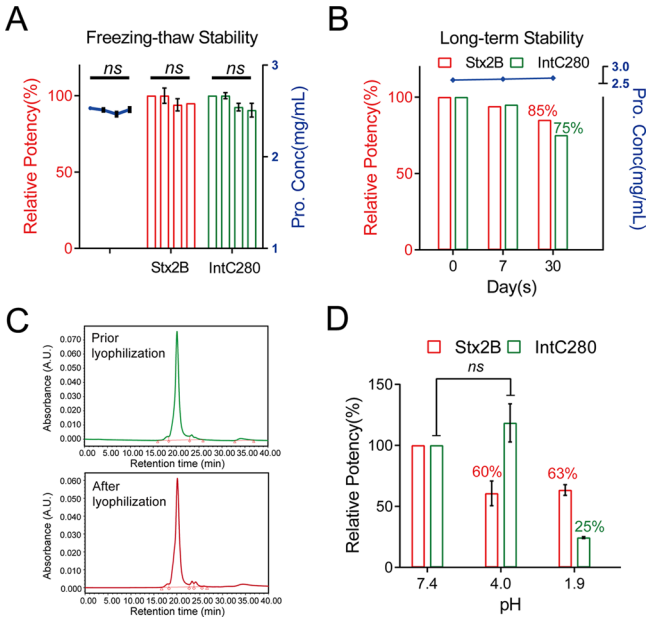

Figure 6. Stability of the bispecific neutralizer to storage conditions and pH extremes. Protein concentration (blue), Stx2B binding (red), and IntC280 binding (green) of siNb were determined after three freezing-thaw cycles at −80 °C (A) or long-term storage at 4 °C (B). (C) SEC analysis of siNb before lyophilization and after lyophilization and redissolved in the same volume. (D) Binding capability of siNb to Stx2B and IntC280 in different buffers at pH of 7.4, 4.0, and 1.9.

After storage of siNb at 4 °C for up to 30 days, no significant protein degradation was detected and each portion of the bispecific nanobody maintained at least 85% of its binding capability for Stx2B and 75% for IntC280 (Figure 6B). The stability of siNb to lyophilization was determined by the SEC analysis. As shown by the SEC profile (Figure 6C), there were no significant changes in the retention time and percentage of siNb between samples before and after lyophilization. Moreover, no aggregate corresponding to any multimeric siNb was detected. As the promising potential of a nanobody for inhalable and oral administration against respiratory virus infections, we believe that a nanobody could also be an ideal therapeutic and preventive in the case of STEC infections that initiate in the intestinal mucosa.[33−35] In this regard, we further determined the antigen binding capability of siNb at pH extremes simulating the gastrointestinal environment. As shown in Figure 6D, siNb retained at least 60% of its binding capability to Stx2B under both conditions of pH 4.0 and 1.9. On the other side, the binding of siNb to IntC280 was not altered at pH 4.0 and it still maintained at least 25% of this capability at pH 1.9 although a sharp drop was seen. These data suggest that siNb has excellent stability to be further developed as a STEC prophylactic for oral or inhalable administration.[34−36]

CONCLUSIONS

In conclusion, we constructed a bispecific neutralizer for STEC by genetically fusing together two nanobody modules capable of blocking the binding of Shiga toxin and Intimin to their respective host receptors. The recombinant neutralizer can be easily fabricated in conventional *E. coli* expression systems at relatively low cost and high yield after optimizing the fermentation conditions. Importantly, each of the module from the bispecific neutralizer showed increased antigen binding capability and was able to individually function in the presence of both antigens simultaneously. Moreover, the neutralizer was able to function at pH extremes simulating the gastrointestinal environment and showed high stability under harsh storage conditions. These pharmaceutical advantages together should make such a construct a desirable drug candidate especially for STEC infections in the developing world. Although more *in vivo* studies have to be performed to validate the protection and therapeutic potential of this construct to STEC challenging, this work provides a novel and practical strategy for drug development to combat STEC infections.

METHODS

Materials and Reagents. The *E. coli* plasmids for producing recombinant antigens and nanobodies, including Stx2B (pET22b-Stx2B), IntC280 (pET22b-IntC280), TirM (pET22b-TirM), Nb113 (pET22b-Nb113), IB10 (pET22b-IB10), and Nb113-IB10 (pET22b-NI) (Table S1), were prepared with codon optimization by General Biosystems Co. Ltd. (Anhui, China) and the amino sequences corresponding for IB10 and Nb113 were modified from previous publications.[24,32] Nickel protein purification column (HisTrap HP) and desalting column (HiPrep Desalting) were obtained from Jincheng Biological Co. Ltd. (Wuhan, China). Dulbecco's Modified Eagle Medium (DMEM) and McCoy's 5A medium were purchased from GE Healthcare (Shanghai, China). Fetal Bovine Serum (FBS), Penicillin−Streptomycin solution and HisProbe-HRP were purchased from Thermo-Fisher Scientific (Shanghai, China). FSL-Gb3 construct was purchased from Sigma-Aldrich (Shanghai, China). Myc-tag Rabbit Polyclonal antibody and Alexa-488 conjugated Goat anti-Rabbit IgG antibody were purchased from Proteintech (Beijing, China). Cy5-conjugated Goat anti-Rabbit IgG antibody was purchased from Abcam (Shanghai, China). The BCA kit, TMB kit, ECL kit, and all the HRP-conjugated secondary antibodies were purchased from Beyotime (Shanghai, China).

Cell Culture. Human B lymphoblastoid cell lines Raji and Jeko-1, human colon carcinoma cell lines Caco-2 and HT29, human monocytic leukemia cell line THP-1, and human myelogenous leukemia cell line K562 were kept in our lab. Caco-2 and HT29 cells were grown in DMEM medium with 10% fetal bovine serum (FBS) and antibiotics (100 U/mL penicillin and 100 μg/mL streptomycin). Raji, Jeko-1, THP-1, and K562 cells were grown in RPMI 1640 medium with 10% fetal bovine serum (FBS) and antibiotics (100 U/mL penicillin

https://doi.org/10.1021/acsinfecdis.1c00456
ACS Infect. Dis. 2022, 8, 321−329

and 100 μg/mL streptomycin). All cells were cultured in an incubator with humidified atmosphere containing 5% CO_2 at 37 °C.

Protein Expression and Purification. All the proteins used in this work were expressed in *E. coli* BL21(DE3) cells and purified thorough a nickel protein purification column. Briefly, the transformed *E. coli* cells were grown in Luria−Bertani (LB) medium with supplement of ampicillin (100 μg/mL) at 37 °C in a shaking incubator. After the cell density reached at OD_{600} around 0.6, IPTG at a final concentration of 1 mM was added for protein induction overnight at 16 °C. Cells were then harvested by centrifugation at 8000*g* for 5 min. The pellet of cells was resuspended for sonication in a lysis buffer (10 mM Tris-HCl, 300 mM NaCl, pH 7.4). After centrifugation at 9900*g* for 30 min, the supernatant containing target protein was collected and then loaded into a pre-equilibrated HisTrap HP column for nickel affinity purification according to the manufacturer's instructions. After washing with the suggested buffer, the bound proteins were eluted stepwise through an elution buffer supplemented with increasing concentrations of imidazole from 150 mM to 500 mM and 1 mL-fractions were collected for SDS-PAGE analysis. Purified target proteins were desalted using a HiPrep Desalting column and later concentrated using a 3-kDa centrifugal filter unit. Stx2B and IntC280 proteins were also conjugated with a C-terminal biotin using a Sortase A mediated ligation with a biotin peptide (Table S1, GA-biotin) as we described previously.[25] Protein concentrations were determined using a Bicinchoninic acid (BCA) protein assay kit.

ELISA Analysis of the Binding of Nanobodies and Stx2B. The binding capability of the monospecific nanobody NB113 and the bispecific nanobody to Stx2B was compared by ELISA assay. The ELISA 96-well plate was coated with 100 μL of Stx2B (2 μg/mL) in a coating buffer (0.1 M Na_2CO_3, pH 9.6) at 4 °C overnight. Unbound proteins were removed by washing the plate with PBST and then 200 μL of 3% BSA in PBS were added into the plate for blocking at room temperature for 2 h. After a brief washing with PBST, the plate was then incubated with 100 μL of NB113 or the bispecific nanobody at concentrations as indicated in the corresponding figures at room temperature for 2 h. After washing the plate three times with PBST, 100 μL of HisProbe-HRP (1 μg/well) was added and incubated at room temperature for additional 0.5 h. After three times washing with PBST, the HRP-based signal was developed by adding 100 μL/well TMB substrate for about 10 min and then quenched with 100 μL/well H_2SO_4 (2 M). The absorbance was recorded in a microplate reader at 450 nm. To determine the binding of the bispecific nanobody to Stx2B in the presence of IntC280, the same Stx2B-coated plate was incubated with 100 μL of Bio-IntC280 (2 μg/mL) as a negative control or Bio-IntC280 preincubated with the nanobodies at concentration of 250 nM. All the other steps were the same as described above except for that streptavidin-conjugated HRP (100 μL, 1 μg/mL) was used to detect Bio-IntC280.

ELISA Analysis of the Binding of Nanobodies to IntC280. The binding capability of the monospecific nanobody IB10 and the bispecific nanobody to IntC280 was compared similarly as described for Stx2B. In this case, the ELISA 96-well plate was coated with 100 μL of IntC280 (2 μg/mL) and the binding of IB10 and the bispecific nanobody was determined using HisProbe-HRP. To determine the binding of the bispecific nanobody to IntC280 in the presence of Stx2B, the same IntC280-coated plate was incubated with 100 μL of Bio-Stx2B (2 μg/mL) as a negative control or Bio-Stx2B preincubated with the bispecific nanobody at concentration of 50 nM. Streptavidin-conjugated HRP (100 μL, 1 μg/mL) was used to detect Bio-Stx2B accordingly.

Pull-down Assay. The direct and simultaneous binding of bispecific nanobody to Stx2B and IntC280 was also determined by a pulldown assay. Briefly, streptavidin-conjugated magnetic beads (200 μg) were washed three times with PBST and then incubated with 50 μL Bio-Stx2B (0.5 mg/mL) in a PBS (pH 7.4) buffer containing 0.1% BSA. After incubation at room temperature for 1 h, unbound proteins were removed by washing the beads again three times with PBST and then Stx2B-loaded beads were further incubated with 50 μL of bispecific nanobody (1 mg/mL) preincubated with IntC280 (0.5 mg/mL) at room temperature for 1 h. After three times washing with PBST, proteins retained on the beads were directly subjected for SDS-PAGE analysis. In the same vein, Bio-Int280 was first loaded on the beads and the binding of bispecific nanobody and Stx2B was determined accordingly. Beads incubated with PBS were used as a negative control. Free samples of Stx2B, IntC280, and bispecific nanobodies were loaded directly as input control for analysis. The gel was visualized by Coomassie blue staining.

Shiga Toxin Neutralization Assay. The inhibitory effect of nanobodies on the binding of Stx2B to Gb3 was determined using an ELISA type functional assay essentially as we described previously.[15] Briefly, a 96-well plate (Nunc PolySorb) were coated with FSL-Gb3 (5 μg/mL, 100 μL/well) in PBS overnight at 4 °C. The unbound FSL-Gb3 was removed by washing the plate three times with PBS and 200 μL of 3% BSA in PBS was added into each well to block the potential unspecific binding sites at room temperature for 2 h. After brief washing with PBS, the Gb3-coated plate was incubated with 100 μL of Bio-Stx2B (1000 nM) alone as positive control or Bio-Stx2B preincubated with the bispecific nanobody for 0.5 h at concentration as indicated in the context. In addition, various concentrations of BSA were used as negative controls with respect to the bispecific nanobody. After incubation at room temperature for 2 h, the supernatant from each well was removed and the plate was washed three times with PBS. Bio-stx2B bound to Gb3-coated plate was detected using streptavidin-conjugated HRP (100 μL, 1 μg/mL) and the signal was developed same as above ELISA assays. Regarding the neutralization assay in the presence of IntC280 antigen, the bispecific nanobody was first preincubated for 0.5 h with Bio-Stx2B (1000 nM) and IntC280 (6 μM) at concentrations as described in the context and then Bio-Stx2B binding was determined.

IntC280 Neutralization Assay. The inhibitory effect of the bispecific nanobody on the binding of IntC280 to TirM was determined using an ELISA-based functional assay. Briefly, the ELISA 96-well plate was coated with 100 μL TirM (2 μg/mL) in a coating buffer (0.1 M Na_2CO_3, pH9.6) at 4 °C overnight. After washing with PBS, the plate was blocked with 3% BSA in PBS for 2 h and then plate was incubated with 100 μL Bio-IntC280 (1000 nM) or same amount of Bio-IntC280 preincubated with the bispecific nanobodies for 0.5 h at concentration as indicated in the corresponding figure. With further incubation for 2 h and washing, the plate was added with 100 μL streptavidin-conjugated HRP (1 μg/mL) and incubated at room temperature for 0.5 h. The HRP signal was

https://doi.org/10.1021/acsinfecdis.1c00456
ACS Infect. Dis. 2022, 8, 321−329

developed similarly as descried in above ELISA assay. In the case of neutralization assay with the presence of Stx2B antigen, the bispecific nanobody was first preincubated for 0.5 h with Bio-IntC280 (1000 nM) and Stx2B (19 μM) at concentrations as described in the context and then Bio-IntC280 binding was determined.

Flow Cytometry. Stx2B binding to cells was determined by flow cytometry analysis. Briefly, cells were detached and collected from the culture flasks using a trypsin buffer and then resuspended in a flow cytometry buffer (2% BSA in PBS) at a density of 5×10^5 cells/mL. Stx2B was added into 100 μL of the above cell suspension to final concentrations as indicated in the corresponding figure and the mixture was then incubated on ice for 1 h. Same volume of PBS with respect to Stx2B was used as a parallel negative control. In the test of Stx2B inhibition, Stx2B was first preincubated with the bispecific nanobody at indicated concentrations for 0.5 h and then incubated with the cells for additional 1 h. The treated cells were then centrifuged and washed three times with 500 μL of precold PBS. After the last washing, the pellet of cells was resuspended in 100 μL of anti-Myc antibodies (4 μg/mL) premixed with Cy5-conjugated secondary antibody (10 μg/mL) and incubated in dark on ice for additional 1 h. Finally, the cells were washed three times with 500 μL of cold PBS and then resuspended with 200 μL of PBS for binding analysis using an Accuri C6 flow cytometer. The data was analyzed using a FlowJo Software.

Immuno-cytochemistry Analysis. Stx2B binding to cells was also imaged using immuno-cytochemical assay. HT29 cells (5000 cells/well) seeded on sterile coverslips in 24-well plates were first fixed by 4% paraformaldehyde (PFA) for 10 min, and then blocked with 1% BSA in PBS for 1 h. After a brief washing, cells were treated with Stx2B or Stx2B preincubated with the bispecific nanobody at concentrations as indicated in the corresponding figure and incubated at room temperature for 1 h. After three times washing with PBS, 100 μL of anti-Myc antibody (4 μg/mL) preincubated with Alexa488-conjugated secondary antibody (10 μg/mL) was added to the cells for another 1 h. Again, the cells were washed three times with PBS and then treated with a drop of antifade mounting medium (containing 4′,6-diamidino-2-phenylindole (DAPI)). Finally, images were recorded using a fluorescent microscope.

Stability Analysis of the Bispecific Nanobody. For the freezing-thaw stability, the bispecific nanobody (2.6 mg/mL) in PBS was stored at −80 °C. The frozen sample was allowed to thaw out slowly at 4 °C for the following tests or the repeated frozen and totally three freeze−thaw cycles were performed. The binding of those samples to Stx2B or IntC280 was determined using ELISA assay as described above, while the concentrations of those samples were determined using a BCA protein assay kit. For the long-term storage stability, the bispecific nanobody (2.6 mg/mL) in PBS was stored at 4 °C for days as indicated in the corresponding figure and samples were then analyzed same as freezing-thaw stability. For the pH stability, the bispecific nanobody was diluted at 2.6 mg/mL in PBS buffer pH 7.4, acetate buffer pH 4.0 and acetate buffer pH 1.9, respectively. After incubation at room temperature for 2 h, the binding of those samples to Stx2B or IntC280 was determined accordingly as described above. For the lyophilization stability, 100 μL of the bispecific nanobody (2.6 mg/mL) in PBS was freeze-dried using a vacuum freeze drier. The lyophilized powder of the bispecific nanobody was resuspended in 100 μL of PBS and SEC analysis of the postlyophilization and prior-lyophilization samples were performed on the Agilent 1260 HPLC system equipped with a Shodex OHpak SB-805 HQ column with UV detection at 280 nm. Each sample of 100 μL was loaded into the system and the flow rate was set to 0.5 mL/min.

■ ASSOCIATED CONTENT

Supporting Information

The Supporting Information is available free of charge at https://pubs.acs.org/doi/10.1021/acsinfecdis.1c00456.

Amino acid sequences of proteins expressed (Table S1); SEC spectrum of siNb (Figure S1); Multicharge mass spectrum of siNb (Figure S2); SDS-PAGE analysis of all proteins used (Figure S3); Monospecific nanobodies IB10 and Nb113 had no cross-reactivity (Figure S4); Free antigens had no effect on the binding of siNb to the immobilized antigens (Figure S5); Functional analysis of Stx2B and IntC280 (Figure S6); Binding analysis of Stx2B to Gb3 in the serum (Figure S7); Flow cytometry analysis of Stx2B binding to different cell lines (Figure S8); Flow cytometry analysis of the inhibitory effect of siNb on Stx2B attachment to HT29 cells (Figure S9) (PDF)

■ AUTHOR INFORMATION

Corresponding Authors

Roland J. Pieters − *Department of Chemical Biology & Drug Discovery, Utrecht Institute for Pharmaceutical Sciences, Utrecht University, 3584 CG Utrecht, The Netherlands;* orcid.org/0000-0003-4723-3584; Email: r.j.pieters@uu.nl

Jie Shi − *Key Laboratory of Carbohydrate Chemistry & Biotechnology, Ministry of Education, School of Biotechnology, Jiangnan University, 214122 Wuxi, China;* orcid.org/0000-0002-4310-5326; Email: j.shi@jiangnan.edu.cn

Zhimeng Wu − *Key Laboratory of Carbohydrate Chemistry & Biotechnology, Ministry of Education, School of Biotechnology, Jiangnan University, 214122 Wuxi, China;* orcid.org/0000-0001-7583-7268; Email: zwu@jiangnan.edu.cn

Authors

Zhongkai Lu − *Key Laboratory of Carbohydrate Chemistry & Biotechnology, Ministry of Education, School of Biotechnology, Jiangnan University, 214122 Wuxi, China*

Zhicheng Liu − *Key Laboratory of Carbohydrate Chemistry & Biotechnology, Ministry of Education, School of Biotechnology, Jiangnan University, 214122 Wuxi, China*

Xia Li − *Key Laboratory of Carbohydrate Chemistry & Biotechnology, Ministry of Education, School of Biotechnology, Jiangnan University, 214122 Wuxi, China*

Xinfang Qin − *Key Laboratory of Carbohydrate Chemistry & Biotechnology, Ministry of Education, School of Biotechnology, Jiangnan University, 214122 Wuxi, China*

Haofei Hong − *Key Laboratory of Carbohydrate Chemistry & Biotechnology, Ministry of Education, School of Biotechnology, Jiangnan University, 214122 Wuxi, China*

Zhifang Zhou − *Key Laboratory of Carbohydrate Chemistry & Biotechnology, Ministry of Education, School of Biotechnology, Jiangnan University, 214122 Wuxi, China*

Complete contact information is available at:
https://pubs.acs.org/10.1021/acsinfecdis.1c00456

Notes

The authors declare no competing financial interest.

■ ACKNOWLEDGMENTS

This work was supported by the National Natural Science Foundation of China (No. 21907038 and No. 32000904) and the Health and Family Planning Commission of Wuxi, China (No. Z202005). J. Shi was supported by the basic research program of Jiangnan University (No. JUSRP12016) and the innovation and entrepreneurship program of Jiangsu Province. This work was partly enabled by funding from Natural Science Foundation of Jiangsu Province (No. BK20200601), China Postdoctoral Science Foundation (No. BX20200153 and No. 2021M691293) and the 111 Project (No. 111-2-06).

■ REFERENCES

(1) Byrne, L.; Jenkins, C.; Launders, N.; Elson, R.; Adak, G. K. The epidemiology, microbiology and clinical impact of Shiga toxin-producing Escherichia coli in England, 2009−2012. *Epidemiol Infect* **2015**, *143* (16), 3475−87.

(2) Kim, J. S.; Lee, M. S.; Kim, J. H. Recent Updates on Outbreaks of Shiga Toxin-Producing Escherichia coli and Its Potential Reservoirs. *Front. Cell. Infect. Microbiol.* **2020**, *10*, 273.

(3) Buchholz, U.; Bernard, H.; Werber, D.; Bohmer, M. M.; Remschmidt, C.; Wilking, H.; Delere, Y.; an der Heiden, M.; Adlhoch, C.; Dreesman, J.; Ehlers, J.; Ethelberg, S.; Faber, M.; Frank, C.; Fricke, G.; Greiner, M.; Hohle, M.; Ivarsson, S.; Jark, U.; Kirchner, M.; Koch, J.; Krause, G.; Luber, P.; Rosner, B.; Stark, K.; Kuhne, M. German outbreak of Escherichia coli O104:H4 associated with sprouts. *N Engl J. Med.* **2011**, *365* (19), 1763−70.

(4) Frank, C.; Werber, D.; Cramer, J. P.; Askar, M.; Faber, M.; an der Heiden, M.; Bernard, H.; Fruth, A.; Prager, R.; Spode, A.; Wadl, M.; Zoufaly, A.; Jordan, S.; Kemper, M. J.; Follin, P.; Muller, L.; King, L. A.; Rosner, B.; Buchholz, U.; Stark, K.; Krause, G.; Team, H. U. S. I. Epidemic profile of Shiga-toxin-producing Escherichia coli O104:H4 outbreak in Germany. *N. Engl. J. Med.* **2011**, *365* (19), 1771−1780.

(5) Bryan, A.; Youngster, I.; McAdam, A. J. Shiga Toxin Producing Escherichia coli. *Clin Lab Med.* **2015**, *35* (2), 247−72.

(6) Joseph, A.; Cointe, A.; Mariani Kurkdjian, P.; Rafat, C.; Hertig, A. Shiga Toxin-Associated Hemolytic Uremic Syndrome: A Narrative Review. *Toxins (Basel)* **2020**, *12* (2), 67.

(7) Bruyand, M.; Mariani-Kurkdjian, P.; Gouali, M.; de Valk, H.; King, L. A.; Le Hello, S.; Bonacorsi, S.; Loirat, C. Hemolytic uremic syndrome due to Shiga toxin-producing Escherichia coli infection. *Med. Mal Infect* **2018**, *48* (3), 167−174.

(8) Hall, G.; Kurosawa, S.; Stearns-Kurosawa, D. J. Shiga Toxin Therapeutics: Beyond Neutralization. *Toxins (Basel)* **2017**, *9* (9), 291.

(9) Muhlen, S.; Dersch, P. Treatment Strategies for Infections With Shiga Toxin-Producing Escherichia coli. *Front. Cell. Infect. Microbiol.* **2020**, *10*, 169.

(10) Obrig, T. G.; Karpman, D. Shiga toxin pathogenesis: kidney complications and renal failure. *Curr. Top Microbiol Immunol* **2011**, *357*, 105−36.

(11) Keir, L. S. Shiga toxin associated hemolytic uremic syndrome. *Hematol Oncol Clin North Am.* **2015**, *29* (3), 525−39.

(12) Melton-Celsa, A. R. Shiga Toxin (Stx) Classification, Structure, and Function. *Microbiol. Spectr.* **2014**, *2* (4), EHEC-0024-2013.

(13) Bergan, J.; Dyve Lingelem, A. B.; Simm, R.; Skotland, T.; Sandvig, K. Shiga toxins. *Toxicon* **2012**, *60* (6), 1085−107.

(14) Hostetter, S. J.; Helgerson, A. F.; Paton, J. C.; Paton, A. W.; Cornick, N. A. Therapeutic use of a receptor mimic probiotic reduces intestinal Shiga toxin levels in a piglet model of hemolytic uremic syndrome. *BMC Res. Notes* **2014**, *7*, 331.

(15) Haksar, D.; Asadpoor, M.; Heise, T.; Shi, J.; Braber, S.; Folkerts, G.; Ballell, L.; Rodrigues, J.; Pieters, R. J. Fighting Shigella by Blocking Its Disease-Causing Toxin. *J. Med. Chem.* **2021**, *64* (9), 6059−6069.

(16) Nishikawa, K.; Matsuoka, K.; Kita, E.; Okabe, N.; Mizuguchi, M.; Hino, K.; Miyazawa, S.; Yamasaki, C.; Aoki, J.; Takashima, S.; Yamakawa, Y.; Nishijima, M.; Terunuma, D.; Kuzuhara, H.; Natori, Y. A therapeutic agent with oriented carbohydrates for treatment of infections by Shiga toxin-producing Escherichia coli O157:H7. *Proc. Natl. Acad. Sci. U. S. A.* **2002**, *99* (11), 7669−74.

(17) Mulvey, G. L.; Marcato, P.; Kitov, P. I.; Sadowska, J.; Bundle, D. R.; Armstrong, G. D. Assessment in mice of the therapeutic potential of tailored, multivalent Shiga toxin carbohydrate ligands. *J. Infect Dis* **2003**, *187* (4), 640−9.

(18) Kulkarni, A. A.; Fuller, C.; Korman, H.; Weiss, A. A.; Iyer, S. S. Glycan encapsulated gold nanoparticles selectively inhibit Shiga toxins 1 and 2. *Bioconjug Chem.* **2010**, *21* (8), 1486−93.

(19) Luz, D.; Chen, G.; Maranhao, A. Q.; Rocha, L. B.; Sidhu, S.; Piazza, R. M. Development and characterization of recombinant antibody fragments that recognize and neutralize in vitro Stx2 toxin from Shiga toxin-producing Escherichia coli. *PLoS One* **2015**, *10* (3), e0120481.

(20) Luz, D.; Amaral, M. M.; Sacerdoti, F.; Bernal, A. M.; Quintilio, W.; Moro, A. M.; Palermo, M. S.; Ibarra, C.; Piazza, R. M. F. Human Recombinant Fab Fragment Neutralizes Shiga Toxin Type 2 Cytotoxic Effects in vitro and in vivo. *Toxins (Basel)* **2018**, *10* (12), 508.

(21) Moxley, R. A.; Francis, D. H.; Tamura, M.; Marx, D. B.; Santiago-Mateo, K.; Zhao, M. Efficacy of Urtoxazumab (TMA-15 Humanized Monoclonal Antibody Specific for Shiga Toxin 2) Against Post-Diarrheal Neurological Sequelae Caused by Escherichia coli O157:H7 Infection in the Neonatal Gnotobiotic Piglet Model. *Toxins (Basel)* **2017**, *9* (2), 49.

(22) Tremblay, J. M.; Mukherjee, J.; Leysath, C. E.; Debatis, M.; Ofori, K.; Baldwin, K.; Boucher, C.; Peters, R.; Beamer, G.; Sheoran, A.; Bedenice, D.; Tzipori, S.; Shoemaker, C. B. A single VHH-based toxin-neutralizing agent and an effector antibody protect mice against challenge with Shiga toxins 1 and 2. *Infect. Immun.* **2013**, *81* (12), 4592−603.

(23) Mejias, M. P.; Hiriart, Y.; Lauche, C.; Fernandez-Brando, R. J.; Pardo, R.; Bruballa, A.; Ramos, M. V.; Goldbaum, F. A.; Palermo, M. S.; Zylberman, V. Development of camelid single chain antibodies against Shiga toxin type 2 (Stx2) with therapeutic potential against Hemolytic Uremic Syndrome (HUS). *Sci. Rep.* **2016**, *6*, 24913.

(24) Bernedo-Navarro, R. A.; Romao, E.; Yano, T.; Pinto, J.; De Greve, H.; Sterckx, Y. G.; Muyldermans, S. Structural Basis for the Specific Neutralization of Stx2a with a Camelid Single Domain Antibody Fragment. *Toxins (Basel)* **2018**, *10* (3), 108.

(25) Liu, J.; Hong, H.; Shi, J.; Xie, Y.; Lu, Z.; Liu, Z.; Zhou, Z.; Bian, Z.; Huang, Z.; Wu, Z. Dinitrophenol-mediated modulation of an anti-PD-L1 VHH for Fc-dependent effector functions and prolonged serum half-life. *Eur. J. Pharm. Sci.* **2021**, *165*, 105941.

(26) Broekgaarden, M.; van Vught, R.; Oliveira, S.; Roovers, R. C.; van Bergen en Henegouwen, P. M.; Pieters, R. J.; Van Gulik, T. M.; Breukink, E.; Heger, M. Site-specific conjugation of single domain antibodies to liposomes enhances photosensitizer uptake and photodynamic therapy efficacy. *Nanoscale* **2016**, *8* (12), 6490−4.

(27) Xiang, Y.; Nambulli, S.; Xiao, Z.; Liu, H.; Sang, Z.; Duprex, W. P.; Schneidman-Duhovny, D.; Zhang, C.; Shi, Y. Versatile and multivalent nanobodies efficiently neutralize SARS-CoV-2. *Science* **2020**, *370* (6523), 1479−1484.

(28) Sun, D.; Sang, Z.; Kim, Y. J.; Xiang, Y.; Cohen, T.; Belford, A. K.; Huet, A.; Conway, J. F.; Sun, J.; Taylor, D. J.; Schneidman-Duhovny, D.; Zhang, C.; Huang, W.; Shi, Y. Potent neutralizing nanobodies resist convergent circulating variants of SARS-CoV-2 by targeting diverse and conserved epitopes. *Nat. Commun.* **2021**, *12* (1), 4676.

(29) Melton-Celsa, A.; Mohawk, K.; Teel, L.; O'Brien, A. Pathogenesis of Shiga-toxin producing escherichia coli. *Curr. Top Microbiol Immunol* **2011**, *357*, 67−103.
(30) Ruano-Gallego, D.; Yara, D. A.; Di Ianni, L.; Frankel, G.; Schuller, S.; Fernandez, L. A. A nanobody targeting the translocated intimin receptor inhibits the attachment of enterohemorrhagic E. coli to human colonic mucosa. *PLoS Pathog* **2019**, *15* (8), e1008031.
(31) Bielaszewska, M.; Mellmann, A.; Zhang, W.; Kock, R.; Fruth, A.; Bauwens, A.; Peters, G.; Karch, H. Characterisation of the Escherichia coli strain associated with an outbreak of haemolytic uremic syndrome in Germany, 2011: a microbiological study. *Lancet Infect Dis* **2011**, *11* (9), 671−6.
(32) Ruano-Gallego, D.; Fraile, S.; Gutierrez, C.; Fernandez, L. A. Screening and purification of nanobodies from E. coli culture supernatants using the hemolysin secretion system. *Microb. Cell. Fact.* **2019**, *18* (1), 47.
(33) Haworth, R.; Boyle, M.; Edwards, P.; Gupta, R.; Fagg, R.; Karantabias, G.; Price, M. Preclinical Safety Assessment of 2 Inhaled Single-Domain Antibodies in the Cynomolgus Monkey. *Toxicol Pathol* **2021**, *49* (2), 296−314.
(34) Gai, J.; Ma, L.; Li, G.; Zhu, M.; Qiao, P.; Li, X.; Zhang, H.; Zhang, Y.; Chen, Y.; Ji, W.; Zhang, H.; Cao, H.; Li, X.; Gong, R.; Wan, Y. A potent neutralizing nanobody against SARS-CoV-2 with inhaled delivery potential. *MedComm (Beijing)* **2021**, *2* (1), 101−113.
(35) Nambulli, S.; Xiang, Y.; Tilston-Lunel, N. L.; Rennick, L. J.; Sang, Z.; Klimstra, W. B.; Reed, D. S.; Crossland, N. A.; Shi, Y.; Duprex, W. P. Inhalable Nanobody (PiN-21) prevents and treats SARS-CoV-2 infections in Syrian hamsters at ultra-low doses. *Sci. Adv.* **2021**, DOI: 10.1126/sciadv.abh0319.
(36) Virdi, V.; Palaci, J.; Laukens, B.; Ryckaert, S.; Cox, E.; Vanderbeke, E.; Depicker, A.; Callewaert, N. Yeast-secreted, dried and food-admixed monomeric IgA prevents gastrointestinal infection in a piglet model. *Nat. Biotechnol.* **2019**, *37* (5), 527−530.

https://doi.org/10.1021/acsinfecdis.1c00456
ACS Infect. Dis. 2022, 8, 321−329